

¹ **Effects of Anomalous Electron Heating in simulations
of the March 17, 2013 Geomagnetic Storm**

M. Wiltberger,¹ V. Merkin,² B. Zhang,¹ F. Toffletto,³ M. Oppenheim,⁴ W. Wang,¹ J. G. Lyon,⁵ J. Liu,¹ and Y Dimant⁴

Corresponding author: M. Wiltberger, National Center for Atmospheric Research, High Altitude Observatory, 3080 Center Green, Boulder, CO 80301 (wiltbemj@ucar.edu)

¹High Altitude Observatory, National
Center for Atmospheric Research, Boulder,
Colorado, USA.

²Applied Physics Laboratory, Johns
Hopkins University, MD, USA.

³Department of Physics and Astronomy,
Rice University, TX, USA.

⁴Center for Space Physics, Boston
University, Boston, Massachusetts, USA

⁵Department of Physics and Astronomy,
Dartmouth College, Hanover, NH, USA.

³ **Abstract.** Examines the impacts of including Anomalous Electron Heat-
⁴ ing (AEH) in simulations of to the geomagnetic storm that occurred on 17
⁵ March 2013. We see many cool things.

1. Introduction

6 Initial drafting of this section has been assigned to Meers and Slava.

2. Simulation Setup

7 This study focuses on using the geomagnetic storm that occurred on 17 March 2013
8 as a case study for two new features of the LFM-RCM geospace model. As previously
9 discussed the LFM-RCM model combines the Lyon-Fedder-Mobarry MHD model of the
10 magnetosphere with the Rice Convection Model of the inner magnetosphere and the
11 Mangetosphere-Ionosphere Coupler Solver of ionospheric electrodynamics to provide a
12 tightly coupled model of the geospace system. *Pembroke et al.* [2012] describes in detail
13 the basic process of coupling these three models together during idealized solar wind con-
14 ditions with modest solar wind driving and no dipole tilt. Section 2.1 describes how this
15 approach has been modified to include realistic solar wind conditions, including nonzero
16 IMF B_Y , as well as variations in the Earth's dipole tilt. *Merkin et al.* [2005] implemented
17 an adjustment to the ionospheric conductances based upon the theoretical analysis of the
18 Farley-Buneman instability (FBI) conducted by *Dimant and Milikh* [2003]. This capabil-
19 ity has not be widely used in LFM simulations, but is being made part of the LFM-RCM
20 geospace model. Section 2.2 discusses how both the Anomalous Electron Heating (AEH)
21 and Non-Linear Current (NLC) aspects of the FBI are implemented in the MIX portion
22 of the LFM-RCM model. In the final section of the portion of the paper we present the
23 solar wind conditions present during the 17 March 2013 geomagnetic storm and document
24 the specific details of the LFM-RCM simulation chosen for this event study.

2.1. LFM-RCM

25 *Pembroke et al.* [2012] provides a detailed description of the coupling process between the
26 LFM, MIX and RCM models for simulations of geospace. Since that study used idealized
27 solar wind conditions with no dipole tilt after reviewing the basics of the LFM-RCM
28 coupling this section will address the changes made to coupling infrastructure needed to
29 allow model to work for realistic solar wind conditions and dipole tilts.

30 The fundamental aspect of the model coupling is an exchange of magnetic field and
31 plasma information in the inner magnetosphere to RCM from LFM and then an update
32 of the plasma information from RCM to the LFM. The MIX model is providing iono-
33 spheric potential information to both the LFM and RCM models. All of the exchanges
34 use the Center for Integrated Space Weather Modeling (CISM) *Goodrich et al.* [2004] cou-
35 pling infrastructure and that infrastructure is utilized in the update version. To transfer
36 information from the LFM to the RCM it computes time averages of the pressure, density
37 and magnetic field over an exchange interval. This intermediate grid is then used to calcu-
38 lated field line-averaged pressure and density for positions in the RCM's ionospheric grid.

39 A key innovation of the *Pembroke et al.* [2012] was the implementation of the plasma- β
40 methodology for setting the location of the outer boundary of the RCM. This switch,
41 which essentially prevented the RCM from computing regions with large flows, remains
42 active in the storm simulations we present in this paper. The averaged fields are interpo-
43 lated onto an intermediate regular Cartesian grid. After the RCM computes its plasma
44 pressures and densities these values are transferred back to the LFM once again using
45 the intermediate grid. The RCM density model includes a modifications to a fit of static
46 plasmasphere model of *Gallagher et al.* [2000]. At this time we have not implemented a

47 dynamic plasmasphere calculation, but that is logical next step for improvement of the
48 coupled model. Another set of field line traces from the RCM ionospheric grid points are
49 used to determine the local values on intermediate grid and than those values are inter-
50 polated to LFM grid points. The mapping back to LFM assumes that the distribution
51 of plasma density and pressure is constant along field lines. As before the RCM values
52 do not immediately replace the LFM values, instead they bled into the LFM over the
53 exchange time interval. It is important to note that the previous work used a 1-minute
54 exchange interval as a balance between speed and accuracy. For strong solar wind driving
55 conditions we have found it necessary to reduce the coupling interval to 15-seconds.

56 The first major modification to the previous coupling efforts is in support of including
57 dipole tilts in the calculation of the coupled model. The LFM-MIX model has long had
58 support for conducting simulations with realistic dipole tilts. This is done by continuing to
59 have the dipole axis of the Earth aligned with the Z-axis of the computational model and
60 inputing the solar wind conditions in SM coordinates. As *Hapgood* [1992] explains the SM
61 coordinate system has the Z-axis parallel to the north magnetic pole and transformation
62 between this coordinate system and the more commonly used GSM coordinate system is
63 simply rotation about the Y-axis by the dipole tilt angle. The cartesian intermediate grid
64 is setup in SM coordinates for the transfer of data to and from the LFM to RCM the
65 ionospheric foot points are transformed from geographic coordinates to SM coordinates
66 using the GEOPACK coordinate transform package. While the RCM typically includes
67 the effects of the corotation potential since this is not enabled in the LFM-MIX simulation
68 these effects are disabled within the RCM when it is coupled to the LFM.

69 The second key modification of the LFM-RCM coupling is how the asymmetries in the
70 ionosphere are addressed. In the MIX module the ionospheric potential for the northern
71 and southern hemispheres are calculated independently. The field-aligned current pat-
72 terns are taken from the global MHD simulation are shared between the hemispheres, but
73 the ionospheric conductances can be different. The first major difference comes from the
74 implementation the EUV conductance model that calculates the local value of the Hall
75 and Pedersen conductance based upon the solar zenith angle and the F107 flux value.
76 We have adapted the model used by AMIE for the MIX module *Richmond* [1992]. The
77 ionospheric conductance model also includes an empirical model for electron precipitation.
78 As described by *Wiltberger et al.* [2009] this model includes modifications of the precipita-
79 tion values based upon the local EUV conductance values allowing the model to simulate
80 seasonal variations of particle precipitation and their impacts on geospace system. On
81 the other hand the RCM assumes that there are no differences between the northern and
82 southern hemispheres.

83 The compromise solution we have adopted for the version of the coupled simulations
84 present here works as follows. The low latitude boundary of the the ionospheric solution
85 for electrodynamic solve is extended equatorward for 45° to 60° colatitude. The 45°
86 boudnary corresponds to dipole mapping of the 2 R_E inner boundary of the MHD solution
87 grid within the LFM. The 60° boundary corresponds to the low latitude boundary for the
88 RCM ionospheric calculation. *Frank - Is the previous statement correct?* For the northern
89 hemisphere the typical low latitude boundary condition of assuming that potential is
90 zero is used. The northern hemispheric values for the potential as well as the average
91 energy and flux of precipitating electrons are then stored for latter passage to the RCM

for its calculation. The computation of the southern hemisphere potential is done down 45° with the low latitude boundary value being set of the potential obtained from the northern hemisphere at that location. By setting the southern hemisphere boundary with the northern hemisphere values we are attempting ensure that closed field lines in the calculation have the same potential values. *Slava and Frank - Is that the best way to describe the motivation for this coupling approach? Also, should we address why we aren't passing any kind of aggregate flux or conductance information to the RCM calculation.*

As a quick side note we take a moment to compare our approach that utilized by the Space Weather Modeling Framework Tóth *et al.* [2005] to couple the MHD magnetosphere solution to inner magnetosphere models. De Zeeuw *et al.* [2004] did the initial work coupling the RCM with the BATS-R-US magnetosphere solution. Like us they used field line tracing to compute flux tube quantities for transfer between the two components and also assume the plasma parameters are constant along field lines. They support coupling intervals between 10 seconds to 10 minutes with coupling time between models with balance being driving by the strength of convection within the event being simulated. This initial work was done for simulations with no dipole tilts and uniform ionospheric conductances. Welling and Ridley [2010] presents validation studies comparing the magnetic field and plasma parameters for a set of geomagnetic storms. While these results clearly include the effects of dipole tilts and particle precipitation effects the study does not provide any details on how these conditions are handled in the coupled model. More recently Glocer *et al.* [2013] documented the two-way coupling of the Comprehensive Ring Current Model (CRCM) with the BATS-R-US global magnetosphere model, while they presented results for 22 July 2009 geomagnetic storm the paper does not discuss the details of how dipole

₁₁₅ tilt are addressed. *Frank and Slava - I thought this was a worth while addition here and*
₁₁₆ *not in the introduction since it concentrates on coupling details. Am I being to harsh in*
₁₁₇ *my language about not discussing how the dipole tilt is addressed? I'm not aware of any*
₁₁₈ *OpenGGCM publications with RCM. If I've missed something please let me know.*

2.2. FBI Implementation

₁₁₉ *Dimant and Oppenheim [2011] developed a model for including the effects that plasma*
₁₂₀ *turbulence can have on E-region conductivities in regions of strong DC electric fields. This*
₁₂₁ *tublence can drive nonlinear currents and have strong anomalous electron heating of the*
₁₂₂ *plasma. Both these effects can enhance the conductivity. Their model provides correction*
₁₂₃ *factors for the conductivities that we have implemented into the MIX module.*

₁₂₄ *Meers and Yakov - Please insert a paragraph or two with more background information.*
₁₂₅ *In particular, I need justification for why we are only applying this regions with E greater*
₁₂₆ *than 35 mV/m*

₁₂₇ Inside the MIX module we have implemented the following conductivity correction
₁₂₈ terms. In regions where the electric field is greater than 35 mV/m we have implemented,

$$\Sigma_P^{FBI} = \Sigma_P^O(1 + 0.01(E - 35) + 1.3e10^{-5}(E - 35)^2), \quad (1)$$

₁₂₉ as the calculation for the FBI modified conductivity, Σ_P^{FBI} . In Equation 1 E is the
₁₃₀ ionospheric electric field in mV/m and Σ_P^O is the Pedersen conductivity obtained from the
₁₃₁ baseline ionospheric model and includes both the EUV and electron precipitation terms.
₁₃₂ This multiplier includes the effect of the temperature driven recombination reduction as
₁₃₃ well as the that of nonlinear current. The FBI modified Hall conductivity, Σ_H^{FBI} , is simply

$$\Sigma_H^{FBI} = \Sigma_H^O(1 + 0.01172(E - 35) - 1.207e10^{-5}(E - 35)^2), \quad (2)$$

where Σ_H^O is the baseline Hall conductivity. Figure 1 shows the effects of these multipliers over a range electric fields. The Pedersen multiplier (blue curve) is nearly linear over the range from 35-200 mV/m reaching a peak value of 3.0 at 200 mV/m. The Hall multiplier has a negative coefficient on the squared term and so falls off more dramatically at higher values of the electric field. It reaches a peak value of 2.3 at 200 mV/m. *Meers and Yakov - Not sure if the figure adds much, but I'm happy to include it.*

2.3. 17 March 2013 Simulation

On 17 March 2013 an interplanetary coronal mass ejection arrived at the Earth and drove a significant geomagnetic storm, $D_{ST} < -100$, over the next day. Solar wind conditions obtained from the OMNI dataset were used to drive the LFM-RCM model and those are shown in Figure 2. Prior to the shock preceding the CME the solar wind conditions are fairly typical, namely density 5 cc, velocity 425 km/s, with interplanetary magnetic field (IMF) weak, < 5 nT in magnitude, main in the northward direction. At 05:55 UT a shock is clearly present in the solar wind with V_X GSM reaching -650 km/s and the density increasing to 10 cc. In the next three hours the IMF is variable, with IMF B_Z mainly southward reaching values of -20 nT, but having significant intervals with northward IMF. The Y component of the IMF has similar magnitude in amplitude and appears to have a 180 deg phase shift. After approximately 09:00 UT on the 17th the Y and Z components become more in phase and slowly reduce in amplitude reaching typical values by the end of the day. After about 12:00 UT the solar wind speed slowly begins to decrease reaching a value of about 550 km/s by the end of 17 March.

The LFM-RCM simulations for this interval were run using solar wind conditions from Figure 2. As previously discussed the LFM uses a non-orthogonal spherical mesh for the grid. The simulations conducted here use 106 radial, 96 azimuthal, and 128 polar cells. This quad resolution version of the LFM contains twice as many cells as the results reported by *Pembroke et al.* [2012] initial work with coupling LFM-RCM. The RCM simulations were done on a grid with XX and YY points. The intermediate transfer grid between LFM-RCM used for the field line tracing had a resolution of ZZ. In the MIX ionospheric solution the ionospheric resolution was increased from a 2x2° resolution to 1x1°resolution. The full ionospheric conductance model described by *Wiltberger et al.* [2009] was enabled in the MIX calculations. We ran two sets of simulations. The first hereafter, baseline, used the standard ionospheric model. The second, hereafter AEH, had the AEH implementation discussed in Section 2.2 enabled. The solar wind driving, grid resolution, and all other model parameters are not changed between these two runs.

3. Analysis of results

In this section we examine impact of the using AEH.

3.1. Baseline versus AEH

Initial drafting of this section is assigned to Mike.

Possible figures include

3.2. Comparison with DSMP

Initial drafting of this section has been assigned to Bin.

3.3. Comparison with AMPERE

Initial drafting of this section has been assigned to Mike.

¹⁷² Here will discuss the results and compare them with AMPERE

3.4. Comparison with TS07-D

¹⁷³ Initial drafting of this section has been assigned to Slava.

¹⁷⁴ May include a comparison with pressures in the ring current depending on length

¹⁷⁵ and quality of comparison.

4. Summary and Future Directions

¹⁷⁶ Mike will write this section once the paper is nearly finished.

¹⁷⁷ Our SAPS are the best!

¹⁷⁸ **Acknowledgments.** This material is based upon work supported by NASA grants

¹⁷⁹ XX, YY, and ZZ. The National Center for Atmospheric Research is sponsored by the

¹⁸⁰ National Science Foundation. All model output, simulation codes, and analysis routines

¹⁸¹ are being preserved on the NCAR High Performance Storage System and will be made

¹⁸² available upon written request to the lead author of this publication.

References

¹⁸³ De Zeeuw, D. L., S. Sazykin, R. A. Wolf, T. I. Gombosi, A. J. Ridley, and G. Tóth (2004),

¹⁸⁴ Coupling of a global MHD code and an inner magnetospheric model: Initial results, *J.*

¹⁸⁵ *Geophys. Res.*, 109(A), 12,219.

¹⁸⁶ Dimant, Y. S., and G. M. Milikh (2003), Model of anomalous electron heating in the E

¹⁸⁷ region: 1. Basic theory, *Journal of Geophysical Research*, 108(A), 1350.

¹⁸⁸ Dimant, Y. S., and M. M. Oppenheim (2011), Magnetosphere-ionosphere coupling through

¹⁸⁹ E region turbulence: 2. Anomalous conductivities and frictional heating, *Journal of*

- ¹⁹⁰ *Geophysical Research*, 116(A), A09,304–n/a.
- ¹⁹¹ Gallagher, D. L., P. D. Craven, and R. H. Comfort (2000), Global core plasma model, *J.*
- ¹⁹² *Geophys. Res.*, 105, 18,819.
- ¹⁹³ Glocer, A., M. Fok, X. Meng, G. Tóth, N. Buzulukova, S. Chen, and K. Lin (2013),
- ¹⁹⁴ CRCM + BATS-R-US two-way coupling, *J. Geophys. Res.*, 118(4), 1635–1650.
- ¹⁹⁵ Goodrich, C. C., A. L. Sussman, J. G. Lyon, M. A. Shay, and P. A. Cassak (2004), The
- ¹⁹⁶ CISM code coupling strategy, *J. Atmos. Solar Terr. Phys.*, 66(1), 1469–1479.
- ¹⁹⁷ Hapgood, M. A. (1992), Space physics coordinate transformations - A user guide, *Plane-*
- ¹⁹⁸ *tary and Space Science (ISSN 0032-0633)*, 40, 711–717.
- ¹⁹⁹ Merkin, V. G., G. Milikh, K. Papadopoulos, J. Lyon, Y. S. Dimant, A. S. Sharma,
- ²⁰⁰ C. Goodrich, and M. Wiltberger (2005), Effect of anomalous electron heating on the
- ²⁰¹ transpolar potential in the LFM global MHD model, *Geophysical Research Letters*,
- ²⁰² 32(2), 22,101.
- ²⁰³ Pembroke, A., F. Toffoletto, S. Sazykin, M. Wiltberger, J. Lyon, V. Merkin, and
- ²⁰⁴ P. Schmitt (2012), Initial results from a dynamic coupled magnetosphere-ionosphere-
- ²⁰⁵ ring current model, *J. Geophys. Res.*, 117(A2).
- ²⁰⁶ Richmond, A. D. (1992), Assimilative mapping of ionospheric electrodynamics, *Adv. Space*
- ²⁰⁷ *Res.*, 12(6), 59–68.
- ²⁰⁸ Tóth, G., et al. (2005), Space Weather Modeling Framework: A new tool for the space
- ²⁰⁹ science community, *J. Geophys. Res.*, 110(A), 12,226.
- ²¹⁰ Welling, D. T., and A. J. Ridley (2010), Validation of SWMF magnetic field and plasma,
- ²¹¹ *Space Weather*, 8(3), 03,002.

₂₁₂ Wiltberger, M., R. S. Weigel, W. Lotko, and J. A. Fedder (2009), Modeling seasonal
₂₁₃ variations of auroral particle precipitation in a global-scale magnetosphere-ionosphere
₂₁₄ simulation, *J. Geophys. Res.*, 114(A), 01,204.

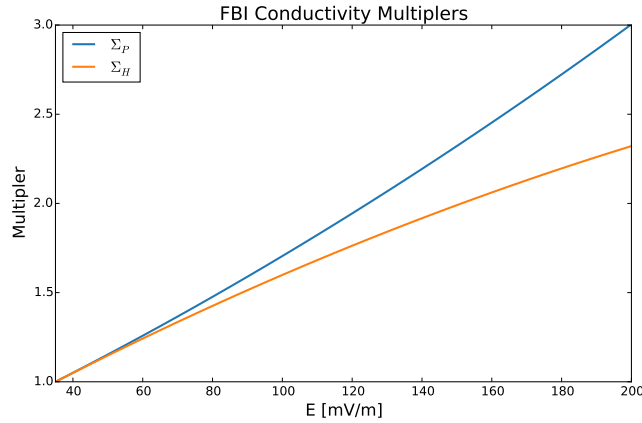


Figure 1. The conductivity multipliers for the FBI effects. The blue curve is for the Pedersen conductivity while the orange curve is for the Hall conductivity. The effects occur for all values above 35 mV/m.

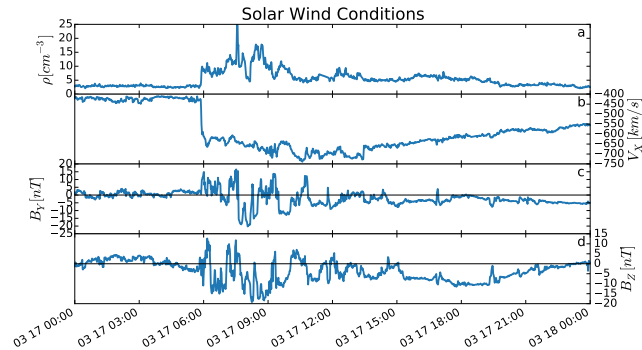


Figure 2. Solar wind and IMF conditions during the 17 March 2013 geomagnetic storm event. Panel a) shows the number density, b) the V_X in GSM coordinates. The IMF GSM Y and Z values are plotted in panels c) and d) respectively.

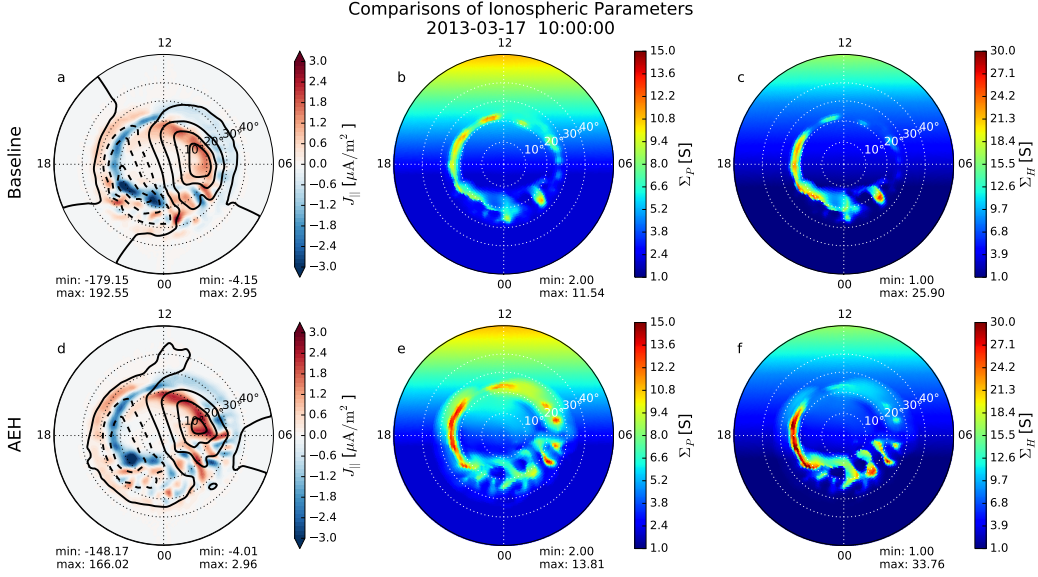


Figure 3. Comparison of FAC and CPCP as well as Pedersen and Hall conductivities for the Baseline and AEH simulations of the 17 March 2016 geomagnetic storm. The top row (panels a-c) contains the results from the baseline simulation while the bottom row (panels d-f) contains the results of the simulation with the AEH enabled. The first column (panels a and d) has the FAC in color with blue being upward and red being downward as well as the CPCP pattern with 20 kV contours. The middle column (panels b and e) contains the Pedersen conductivity. The last column (panels c and f) contains the Hall conductivity. The colorbar for all conductivity plots is the same.

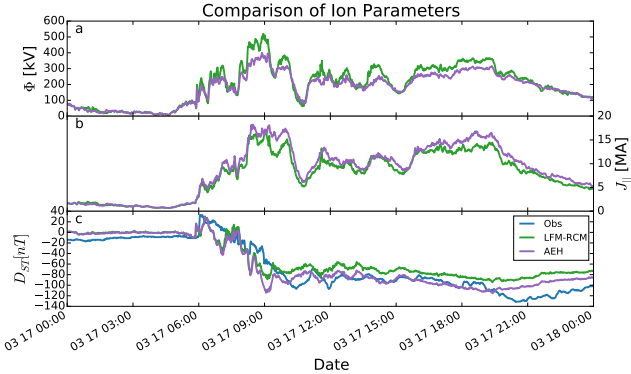


Figure 4. Comparison of the CPCP, FAC, and D_{ST} time series for the storm event for the Northern hemisphere . Panel a at the top shows the CPCP in kV. The middle panel (b) has the integrated FAC. Panel c at the bottom has the D_{ST} index. In each panel the LFM-RCM results are shown with the green line, the AEH results with the purple line. In the bottom panel the D_{ST} obtained from CDAWeb is plotted in blue

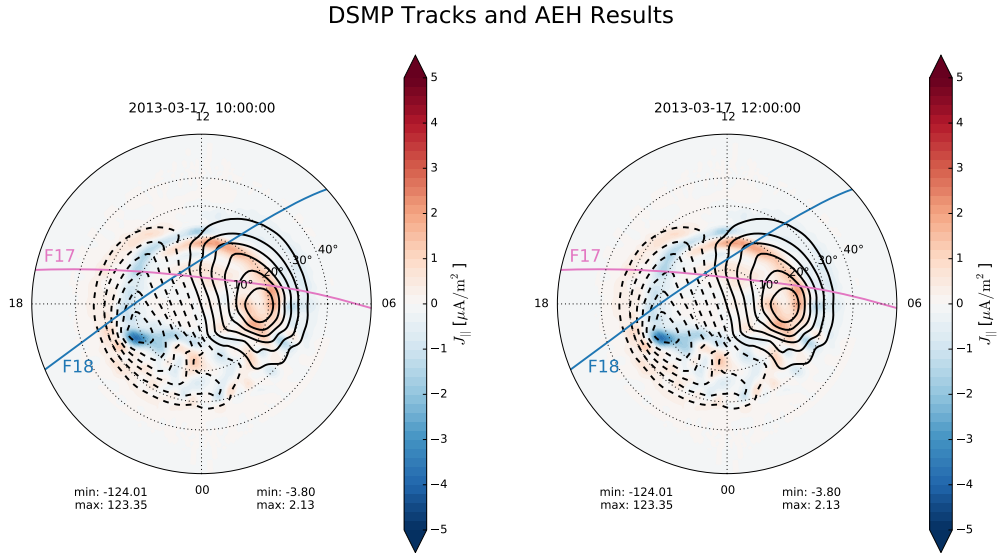


Figure 5. DSMP F17 and F18 trajectories overlaid ontop of AEH FAC and CPCP patterns. Panel a shows the F17 trajectory between 0945 and 1030 UT and the F18 trajectory beteween 1000 and 1045 UT overlaid on top of the AEH simulation results for 10:00UT. Panel b shows the F17 trajectory between 1125 and 1210 UT and the F18 trajectory beteween 1145 and 1230 UT overlaid on top of the AEH simulation results for 12:00UT. In each panel the F17 trajectory is pink and the F18 trajectory is blue.

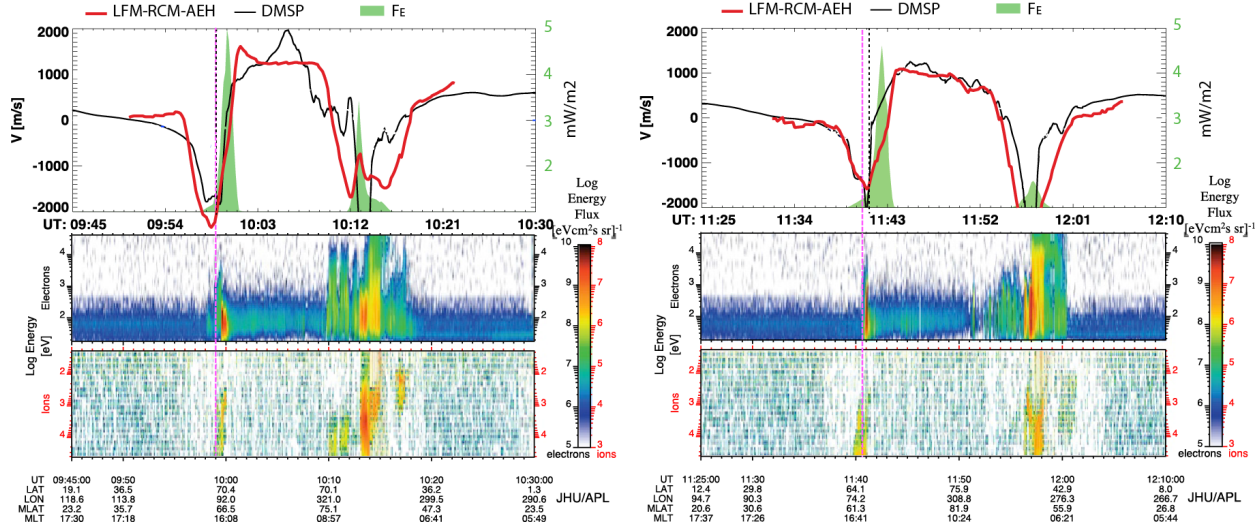


Figure 6. Temporary Figure comparing DMSP F17 results.

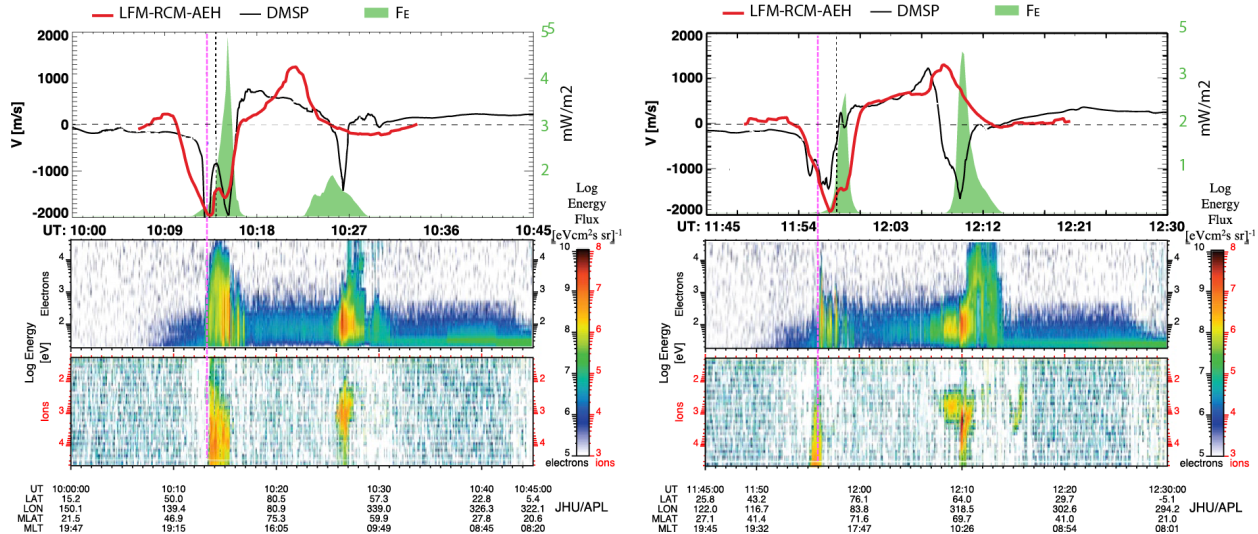


Figure 7. Temporary Figure comparing DMSP F18 results

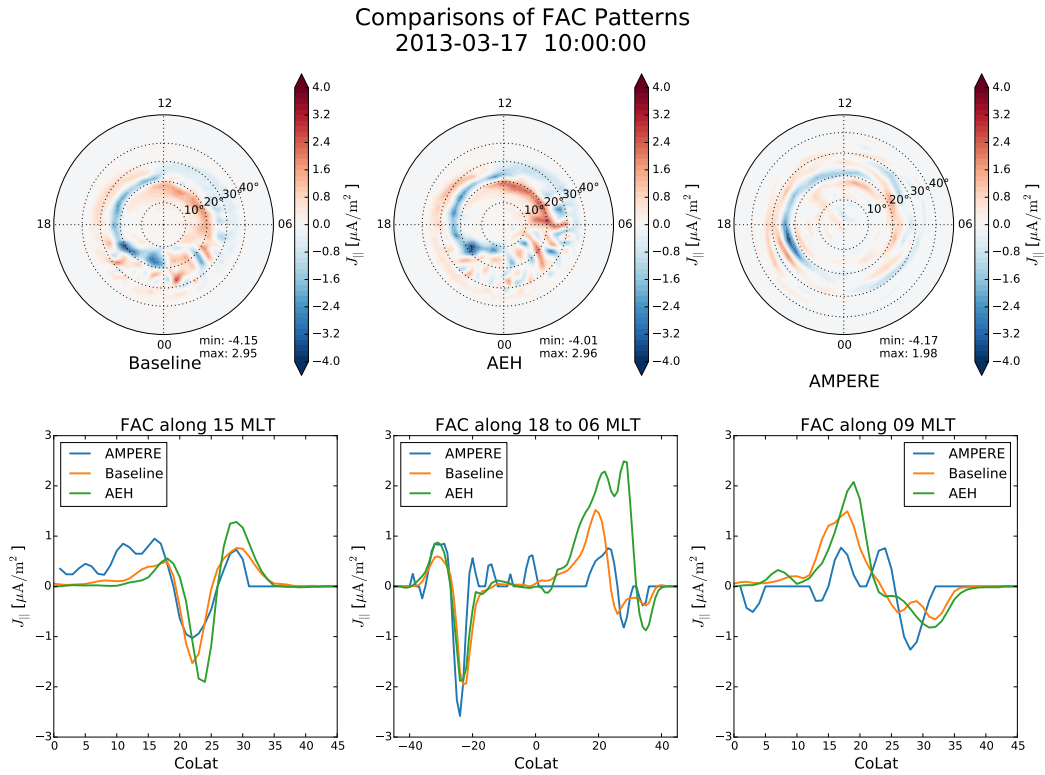


Figure 8. Temporary Figure comparing AMPERE and LFM-RCM

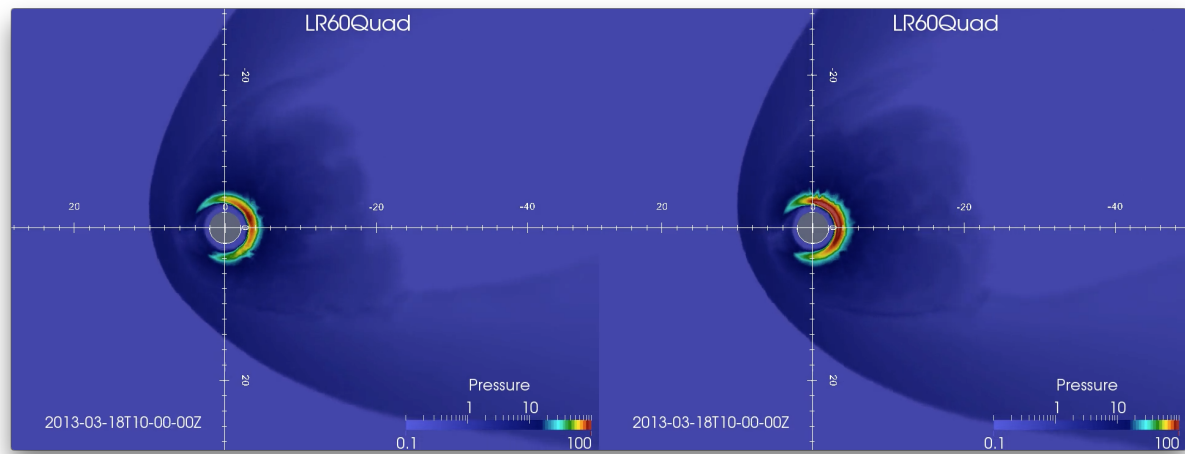


Figure 9. Temporary Figure comparing Baseline and AEH pressures